IEEE Access
Multidisciplinary | Rapid Review | Open Access Journal

Received December 28, 2018, accepted January 9, 2019, date of publication January 21, 2019, date of current version February 14, 2019.

Digital Object Identifier 10.1109/ACCESS.2019.2893894

Optimized Handling Stability Control Strategy for a Four In-Wheel Motor Independent-Drive Electric Vehicle

YONG CHEN, SIZHONG CHEN, YUZHUANG ZHAO, ZEPENG GAO, AND CHANGLONG LI
School of Mechanical Engineering, Beijing Institute of Technology, Beijing 100081, China

Corresponding author: Yuzhuang Zhao (zyz1112@bit.edu.cn)

This work was supported in part by the National Nature Science Foundation of China under Grant 51375046 and Grant 51205021, and in part by the National Key Research and Development Program of China under Grant 2017YFB0102602.

ABSTRACT An optimized handling stability control strategy is put forward aiming at enhancing a four in-wheel independent-drive motors electric vehicle (4WIDEV) performance capable of handling and stability. The optimized control strategy is designed by a hierarchical control structure, which mainly includes vehicle motion controller and vehicle torque distribution controller. Lateral stability controller, in-vehicle motion controller, which yields the generalized force and generalized yaw moment required of the vehicle, is designed into two modes: an instability control mode and a continuous control mode, which mode is activated determining by stability judgment controller based on phase portraits of sideslip angle and yaw rate. When the vehicle state exceeds the stability envelope region, instability control mode based on envelope control is utilized by sliding mode control method, simultaneously controlling the two-vehicle states variables, whereas continuous control mode is performed with adaptive adjustment of the weight parameter according to pre-defined stability degree. The lateral stability controller with adaptive switching two modes exhibits excellent handling stability performance under normal driving conditions, especially under critical conditions, such as on low tire-road adhesion coefficient. The vehicle torque distribution controller assigns driving or regenerative braking torque to four wheels reasonably and efficiently to satisfy the generalized force and the generalize yaw moment acquired by the vehicle motion controller, which synchronously considers the motor output capability and tire friction ellipse constraints while maintains each wheel slip ratio within the stable range. The results in co-simulation experiments based on Carsim and MATLAB/Simulink verify the proposed control strategy, compared with other control strategies, and demonstrate the effective improvement 4WIDEV's performance in terms of handling stability especially under critical conditions.

INDEX TERMS Electric vehicles, in-wheel motor, vehicle handling stability, sliding mode control, independent drive.

I. INTRODUCTION

With the shortage of global petroleum resources, global warming and the aggravation of greenhouse gas emission, electric vehicles (EVs) with a secondary renewable energy source are the development trend and direction of the automotive industry [1]–[3]. As a kind of distributed driving of EVs, the four in-wheel motor independent-drive electric vehicle (4WIDEV) with each motor integrated into each wheel, simplifies the transmission system, possess the capability of the high efficiency of energy [4], [5]. However, some challenges still need to be conquered in energy management, such as battery management and regenerative braking energy recovery [6], [7]. 4WIDEV is driven or braked by four in-wheel motors in a wire-controlled manner, which has the characteristic of fast response and is conducive to the electronization and flexibility of the vehicle chassis system [8]–[10].

In addition, each motor can be controlled independently and accurately, which can fully tap the potential performance to keep the human driver gaining the excellent maneuverability while ensure vehicle handling stability. The system driven

The associate editor coordinating the review of this manuscript and approving it for publication was Mouloud Denai.

by four in-wheel motors (IWMs) is typical over-actuated system and can performs favorable path-tracking flexibility by various fault-tolerant approaches when IWMs encounter different type faults [11]–[13]. However, compared with the internal combustion engine power vehicle, 4WIDEV faces more challenges which are reflected not only in energy management, but also in handling stability and maneuverability control because of the different of structure and control methods, which cannot adopt the methods of controlling internal combustion engine vehicle for 4WIDEV. Extensive researches has been carried out for 4WIDEV by institutes and colleges aiming at improved performance of handling stability [14]–[16].

Hierarchical control structure possesses superior control flexibility and advantages over centralized control structure, which has excellent applicability to deal with nonlinear and over-actuated systems and is extensively adopted in vehicle stability control [10], [12], [17], [18]. Vehicle motion controller serves as first-layer controller to realize vehicle states achieving desired ones while ensures human driver maneuverability [19]–[21]. In the second-layer controller, the torque allocation algorithm quickly and legitimately distributes the command of each actuator in an optimal way [22]. Envelope control, which is a concept that originally applied to control aircraft within a safe region of the state pace, is gradually utilized in vehicle motion control. Envelope control firstly depicts the stability envelope region according to phase portraits of the side slip angle and yaw rate of vehicle ($\beta - r$ phase portraits) or phase planes of the side slip angle and its rate ($\beta - \dot{\beta}$ phase planes), and secondly exerts a corresponding active yaw moment or modifies corrected wheel steer angle to keep vehicle states back within the envelope region when the vehicle states escape the stability envelope [23], [24]. Bobier *et al.* [23] detail accurate mathematical description for safe envelope boundary of $\beta - r$ phase portraits and design a lateral stability controller based on envelope control, preventing the vehicle states from exceeding the envelope boundary by actively correcting the front wheel angle. Ni *et al.* [24] proposed a novel dynamic control concept based on envelope control by generalization desired yaw moment for an autonomous ground vehicle (AGV) equipped with four IWMs and actively front wheel steer system. Erlien *et al.* [25] presented a shared control scheme for electric steer-by-wire vehicle by using two safe driving envelope of obstacle avoidance and stability control constraint. Based on envelope control vehicle motion algorithms express extremely applicability to prevent vehicle state losing its stability [26]. However, that has some limitations and disadvantages, which loses effectiveness and influence for handling stability enhancement when vehicle states stay in the envelope region.

There are also various methodologies, e.g., PID-based [27], fuzzy control (FC), linear quadratic regulator (LQR), model predictive control (MPC) [26], [28] and sliding model control (SMC) [20] methods, are adopted in vehicle motion control to yield generalized forces and/or generalized moment by controlling vehicle reference states respectively. Zhai *et al.* [27] presented an electric stability control algorithm (ESC), in which the $\beta - r$ phase planes is taken as threshold value in terms of safety boundary and the yaw rate is constrained in feasible scope, aims at enhanced stability for 4WIDEV. However, they do not give the weights description of the side slip angle and yaw rate under different vehicle state stability in calculating generalized yaw moment. Yuan *et al.* [26] exploited a new control system for EVs driven by four IWMs where the wheel slip ratio stable region is considered as time-domain in nonlinear MPC for safety reasons and evaluate the multi-objective optimization control with a slack variables' penalty for consideration of infeasible problems in co-simulation and prototyping platform. Wang *et al.* [29] utilized a linear parameter-vary control method to yield the desired yaw moment based on 2-DOF vehicle model, which proves considerable adaptability for 4WIDEV. Zhang *et al.* [12] and Yin *et al.* [18] improved sliding mode control and robust control, respectively, by introducing exponential reaching law or utilizing tire-road adhesion (μ) integrated control techniques for enhancement adaptiveness of parametric uncertainties and un-modeled dynamics. In fact, in the process of selecting parameters in vehicle motion controller design, establishing the model of external interference is also of guiding significance for parameters confirmation. Liu *et al.* [30] increased a lateral stability controller in vehicle motion controller for hybrid EVs driven by eight IWMs, which improves the stability to some extent and confirms the real-time implementation in the hardware-in-loop tests. However, satisfying the lateral force requirements by tracking desired side slip angel indicates high output torque value of motors.

Various torque allocation algorithms, such as active set algorithms and augmented lagrangian methods, have been implemented to satisfy the generalized forces and generalized yaw moment acquired by vehicle motion control, exhibiting outstanding applicability and suitability for over-actuated system driven by 4IWMs [10], [31]–[35]. The torque distribution by recent researches are integrated into constrained control allocation (CA) or multi-objective optimization by coordination and definition of indicators related to vehicle performance. Shuai *et al.* [17] proposed two cost functional indicates for 4WIDEV to minimize the yaw moment demanding error and distributed forces of four wheels with tire-road adhesion μ as a parameter part of weight facts. Liu *et al.* [36] utilized inter-axle torque distribution controller, in which anti-wheel slip and battery power limitation are constrained in optimization torque allocation for novel-axle EVs. Nguyen *et al.* [37] established a shared control authority coordination mechanism in proposed adaptive authority allocation strategy and taken unpredictable driver-automation interaction into account, which is implemented to handle the time-varying driver activity variable with considering condition of the vehicle speed's large variety range. Dizqah *et al.* [38] taken full advantage of over-actuated systems of EVs with four IWMs and proposed analytical solution

of the CA problems to maximizing energy efficiency under the experimental hypothesis. However, due to the complexity of the allocation algorithms, handling obstacles by simplifying constraints while guaranteeing the essential qualifications is crucial for realization of assigning force demands computationally and fast.

Due to the draw back and insufficiency of 4WIDEV in terms of handling stability improvement, the optimized handling stability control strategy in this paper is proposed. the main innovations of whose lie in the following three aspects. (1) The lateral stability controller, built in the vehicle motion controller, is divided into two modes based on the stability judgment controller whose purpose is to determine whether the vehicle is in stable region or not. The continuous mode with adaptive adjustment of the weight parameter is adopted for improvement handling stability of 4WIDEV when in the parallelogram envelope region inside. An approximately related stability degree is constructed based on $\beta - \dot{\beta}$ phase planes, which is taken as a weight fact when we consider that vehicle generalized lateral force is achieved by each tire longitudinal force especially when the vehicle is on low tire-road adhesion. (2) The vehicle's handling stability is guaranteed by instability control model based on envelope control when the vehicle exceeds the parallelogram envelope stability boundary, in which the vehicle the active yaw moment is applied and be returned to the stability envelope inside again. (3) In the vehicle torque distribution controller, by using control allocation under constraints, reference tire longitudinal forces of four wheels are obtained in tire force distribution controller by considering constraints that the amplitude saturation limit of motor torque, friction elliptical circle constraint of tire force. The optimization slip ratio is integrated in tire slip ratio controller generating desired driving or regenerative braking torque while preventing each wheel from exceeding the limitation of optimal slip ratio.

This paper is elaborated in the following several arrangements. Section II shows the basic introduction about structure and parameters of 4WIDEV. Section III describes the optimized handling stability control strategy structure for improvement handling and stability performance of 4WIDEV. The control strategy proposed in a co-simulation environment based on MATLAB/Simulink and Carsim is investigated by three different conditions with or without driver-in-loop and other control strategies are compared in section IV. Conclusions, in section V, are summaries and progress made in this study.

II. WIDEV BASIC STRUCTURE

The structure diagram of 4WIDEV studied in this paper is shown in Fig. 1 which mainly includes motor controller system, energy battery and in-wheel motors. The vehicle control unit controller receives the signals sent by the sensors of steering wheel and acceleration/brake pedal, and sent target instructions to each motor controller and the battery management system (BMS) through CAN bus. The motor controller controls the driving and regenerative braking torque

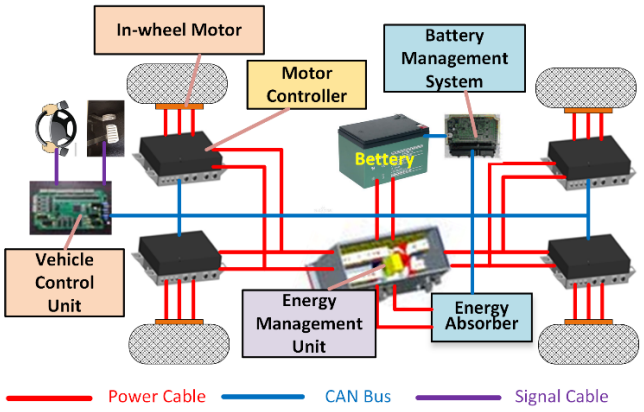

FIGURE 1. Structure diagram of 4WIDEV.

of the motor, so as to ensure the 4WIDEV handling and stability. The energy management unit provides power to each motor by managing the power/energy output of the battery. Motor controller and battery energy management also sent information of battery and in-wheel motor to vehicle controller through CAN bus, which displays some information in the display panel. The basic parameters of 4WIDEV and in-wheel motor are shown in Table 1.

TABLE 1. Basic parameters of 4WIDEV.

Vehicle parameters	Value
Vehicle mass (kg)	1411
Length from the center of gravity (CG) to the front wheel axis (m)	1.04
Length from CG to the front wheel axis (m)	1.56
Tread width (m)	1.48
Tire effective radius (m)	0.3
Height of the center of mass (m)	0.54
Moment of inertia about the Z axis (kg·m2)	2031.4
Rated power (kW)	14
Rated speed (rpm)	800
Rated torque (Nm)	170

III. OPTIMIZED HANDLING STABILITY CONTROL STRATEGY STRUCTURE

The optimized handling stability control strategy proposed for 4WIDEV mainly includes the following modules: vehicle motion controller and vehicle torque distribution controller, as shown in Fig. 2. According to the driver's input, which includes accelerating pedal signal and braking pedal signal, thereby the reference longitudinal speed is obtained. The longitudinal motion controller, in vehicle motion controller, obtains target longitudinal force required in vehicle motion, which realizes the vehicle's actual longitudinal speed tracking reference longitudinal speed. The lateral stability controller can be divided into two modes according to the stability judgment controller. Based on the $\beta - r$ phase portraits, the stability judgment controller judges whether the vehi-

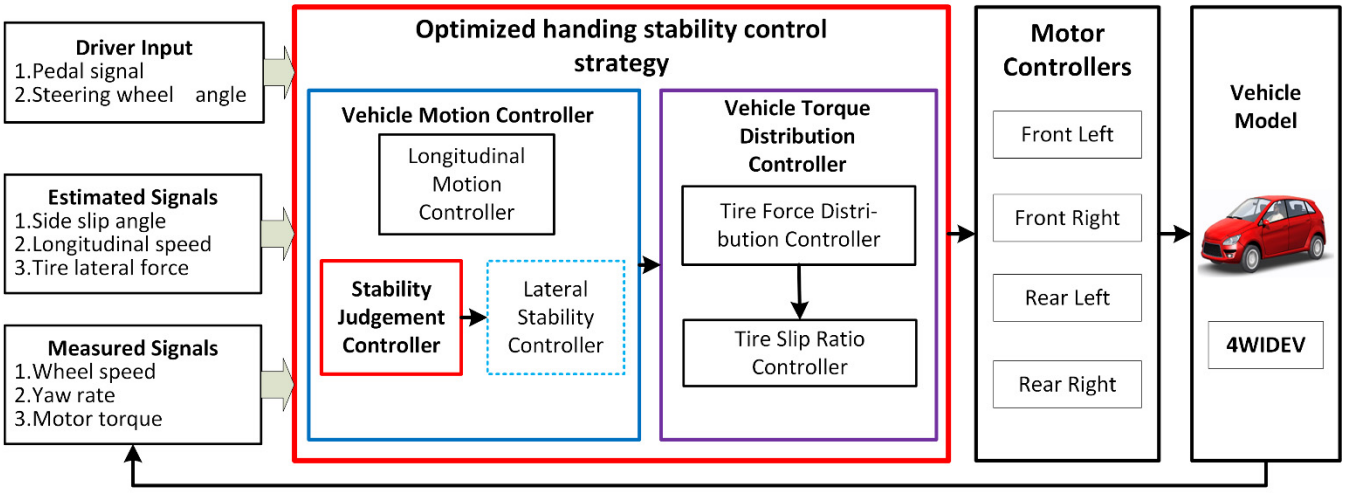

FIGURE 2. Structure of optimized handling stability control strategy.

cle is in stability region or not according to the feedback states of 4WIDEV. If 4WIDEV states are outside the envelope of stability region after the stability judgment controller determining.

The instability control mode based on envelope control will be turned on by using the SMC method and apply an active yaw moment to push 4WIDEV back into the envelope stability region again. Otherwise, the continuous control mode is utilized based on $\beta - \dot{\beta}$ phase planes, which obtains target lateral force and target yaw moment by minimization the error between 4WIDEVs' feedback values (β/r) and corresponding reference ones, respectively. Acquisition of target lateral force is modified by an adaptive adjustment parameter based on approximately definition the degree of vehicle stability. The purpose of the two modes is to ensure the stability of the vehicle when escapes the envelope stability region and to improve the handling stability in envelope stability region, respectively. In addition, the reference state values of 4WIDEV are acquired according to 2DOF-VM and tire-road adhesion coefficient limitation. The vehicle torque distribution controller includes tire force distribution controller and tire slip ratio controller, the purpose of whose realizes the vehicle target longitudinal force F_{Xxd}, target longitudinal force F_{Yxd} and target yaw moment M_{zxd2} (or the target longitudinal force F_{Xxd} and active yaw moment M_{Zxd1}) obtained by the vehicle motion controller converting to the desired driving or regenerative braking torque of each motor T_{dij}. The tire longitudinal force F_{dij} can be allocated optimally, reasonably and rapidly by tire force distribution controller. The tire slip ratio controller can prevent the vehicle losing handling stability from wheel excessive slip by setting the optimal slip ratio limit value when the controller calculates the desired driving or regenerative braking torque of each motor. each motor controller of 4WIDEV receives the desired torque command signals, thus realizing the vehicle's handling and stability control by coordinating the output torque of four in-wheel motors.

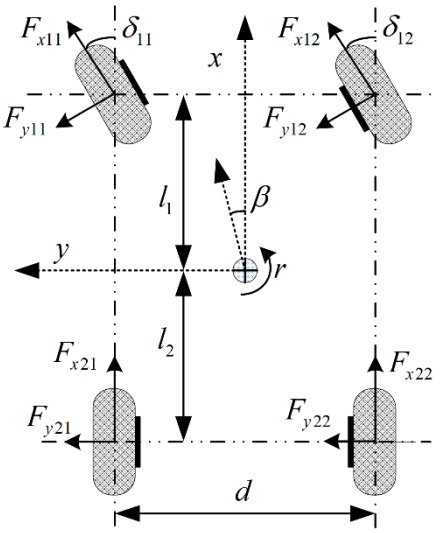

FIGURE 3. Plane movement in vehicle coordinate system.

A. MOTION CONTROLLER

The plane movement of 4WIDEV with front wheel steering in vehicle coordinate system is shown in the Fig. 3. Longitudinal motion of the vehicle reflects longitudinal handling ability of the vehicle to a certain extent. The vehicle's path angle is related to the vehicle yaw angle and the side slip angle, which reflects the lateral stability of the vehicle. The differential equation of vehicle longitudinal, lateral and yaw motions related to vehicle handling and stability can be described as

$$\begin{bmatrix} \dot{v}_x \\ \beta \\ \dot{r} \end{bmatrix} = \begin{bmatrix} v_x \beta r - F_{wind} \\ -r \\ 0 \end{bmatrix} + \begin{bmatrix} \frac{1}{m_v} & 0 & 0 \\ 0 & \frac{1}{m_v v_x} & 0 \\ 0 & 0 & \frac{1}{I_z} \end{bmatrix} \boldsymbol{V} + \boldsymbol{d} \tag{1}$$

where, v_x, β, and r represent the longitudinal speed, the sideslip angle and the yaw rate of the vehicle, respectively. F_{wind} indicates air resistance produced by vehicle body interaction with air, which mainly related to the relative speed of the vehicle and the wind and cannot be ignored especially in the case of large relative speed. m_v and I_z denote the vehicle mass and the moment of inertia of the vehicle around the z axis, respectively. The vector $\boldsymbol{d}$ represents road, sensor noise and high-order dynamic coupling term ignored by external interference from each channel.

$$\boldsymbol{d} = \begin{bmatrix} d_1 \\ d_2 \\ d_3 \end{bmatrix} = \begin{bmatrix} F_R - \dfrac{m_b h_0(\dot{q} + pr)}{m_v} \\ \dfrac{m_b h_0(\dot{p} + qr)}{m_v v_x} \\ \dfrac{I_{zx,b}\dot{p}}{I_z} \end{bmatrix} \tag{2}$$

where, F_R represents the rolling resistance of vehicle. m_b and h_0, respectively, denote the vehicle body mass and vertical distance from vehicle body centroid to roll axis when the vehicle is stationary. $I_{zx,b}$ is moment of inertia relative to x axis and y axis of vehicle body. The vector $\boldsymbol{V}$, consists the total longitudinal, the total lateral force and the total yaw moment acting on the vehicle generated by the tire force between the tire and the ground friction.

$$\boldsymbol{V} = \begin{bmatrix} F_{Xx} + F_{Xy} \\ F_{Yx} + F_{Yy} \\ M_{Zx} + M_{Zy} \end{bmatrix} = \begin{bmatrix} \mathfrak{N}_1 \\ \mathfrak{J}_1 \\ \mathcal{Q}_1 \end{bmatrix} \boldsymbol{F_x} + \begin{bmatrix} \mathfrak{N}_2 \\ \mathfrak{J}_2 \\ \mathcal{Q}_2 \end{bmatrix} \boldsymbol{F_y} \tag{3}$$

where, $\begin{bmatrix} \mathfrak{N}_1 & \mathfrak{J}_1 & \mathcal{Q}_1 \end{bmatrix}^T$ and $\begin{bmatrix} \mathfrak{N}_2 & \mathfrak{J}_2 & \mathcal{Q}_2 \end{bmatrix}^T$ are the matrices determined by trigonometric function of wheel steering angle based on the theoretical mechanics. $\boldsymbol{F_x}$ and $\boldsymbol{F}_y$ column vectors composed of longitudinal force and lateral force of each tire, respectively. These vectors are described as

$$\begin{bmatrix} \mathfrak{N}_1 \\ \mathfrak{J}_1 \\ \mathcal{Q}_1 \end{bmatrix} = \begin{bmatrix} \cos\delta_{11} & \cos\delta_{12} & 1 & 1 \\ \sin\delta_{11} & \sin\delta_{12} & 0 & 0 \\ -\frac{d}{2}\cos\delta_{11} + l_1\sin\delta_{11} & \frac{d}{2}\cos\delta_{12} + l_1\sin\delta_{12} & \frac{d}{2} & \frac{d}{2} \end{bmatrix}$$
$$\begin{bmatrix} \mathfrak{N}_2 \\ \mathfrak{J}_2 \\ \mathcal{Q}_2 \end{bmatrix} = \begin{bmatrix} -\sin\delta_{11} & -sin\delta_{12} & 0 & 0 \\ \cos\delta_{11} & \cos\delta_{12} & 1 & 1 \\ l_1\cos\delta_{11} + \frac{d}{2}\sin\delta_{11} & l_1 cos\delta_{12} + \frac{d}{2}\sin\delta_{12} & -l_1 & -l_2 \end{bmatrix} \tag{4}$$

$$\begin{aligned} \boldsymbol{F_x} &= \begin{bmatrix} F_{x11} & F_{x12} & F_{x21} & F_{x22} \end{bmatrix}^T \\ \boldsymbol{F_y} &= \begin{bmatrix} F_{y11} & F_{y12} & F_{y21} & F_{y22} \end{bmatrix}^T \end{aligned} \tag{5}$$

where δ_{11} and δ_{12}, respectively, represent the wheel angle of the left front wheel and the right front wheel. The alphabet footnote ij ($i \in [1, 2], j \in [1, 2]$) indicates the position of the tire in the vehicle. i in the tire force footnote in the vector represents the i axis of a vehicle, while $j = 1$ or $j = 2$ indicate the left or right side of the vehicle wheel, respectively. The footnote in the following letters follows the same rule.

Since the three state variables (v_x, β, and r) can be estimated or measured and the control input vectors are decoupled from each other [37], [39], the multi input-multi output (MIMO) system can be divided into three single input-single output (SISO) systems.

$$\dot{x}_i = f_i(x, t) + g_i(x, t)u_i \tag{6}$$

where, x_1, x_2, and x_3 denote longitudinal speed v_x, side slip angle of the vehicle β and yaw rate r, respectively. Both f_i and g_i, respectively, include nominal terms ($\hat{f}_i$, $\hat{g}_i$) and uncertainties (Δf_i, Δg_i).

$$\begin{aligned} f_i &= \hat{f}_i + \Delta f_i \\ g_i &= \hat{g}_i + \Delta g_i \end{aligned} \tag{7}$$

where,

$$\begin{aligned} \hat{f} &= \begin{bmatrix} \hat{f}_1 & \hat{f}_2 & \hat{f}_3 \end{bmatrix}^T = \begin{bmatrix} x_2 x_3 & -x_1 x_3 & 0 \end{bmatrix}^T \\ \hat{g} &= \begin{bmatrix} \hat{g}_1 & \hat{g}_2 & \hat{g}_3 \end{bmatrix}^T = \begin{bmatrix} 1/m_v & 1/m_v & 1/I_z \end{bmatrix}^T \end{aligned} \tag{8}$$

Uncertainty and control input of each SISO system, are in the same channel. We assume that the error of f_i and g_i caused by external interference noise signal and modeling uncertainty has its boundary.

$$\begin{cases} |\Delta f_i| = \left| f_i - \hat{f}_i \right| \le F_i \\ \vartheta_i^{-1} \le g_i / \hat{g}_i \le \vartheta_i \end{cases} \tag{9}$$

where,$\vartheta_i = \sqrt{g_{imax}}/g_{imin}$. We assume that the variation range of vehicle mass and yaw moment of inertia is $m_v \in [\, m_{vmin}\ m_{vmax}\,]$, $I_z \in [\, I_{zmin}\ I_{zmax}\,]$. The nominal quantity can be set as follows: $\hat{m}_v = [m_{vmin} m_{vmax}]$, $I_z = \sqrt{I_{zmin} I_{zmax}}$.

1) LONGITUDINAL MOTIOIN CONTROLLER

The longitudinal force in vehicle motion is calculated by longitudinal motion controller, based on feedback control, designed by SMC method, which is realized by longitudinal speed of the vehicle tracking to reference longitudinal speed [10], [16]. Feedback control provides a way for vehicle state relating to handling stability tracking to reference state in real time, which is widely used in vehicle dynamics control [37], [38].

The relative degree of freedom of each control output channel is one. For longitudinal speed, sideslip angle and yaw rate of vehicle controlling and tracking, the selected sliding surface determines the desired dynamic quality of the vehicle system. We select the sliding surface of the longitudinal speed tracking reference longitudinal speed.

$$S_1 = x_1 - x_1^r \tag{10}$$

where, x_1 and x_1^r refer to feedback state of vehicle longitudinal speed and the vehicle's reference longitudinal speed, respectively. The vehicle reference longitudinal speed is determined by the pedal strength and initial speed.

$$x_1^r = v_x^r = v_0 + \int_{t_0}^{t} a_x dt \tag{11}$$

where, v_0 is the initial speed at t_0. a_x is the strength of acceleration/brake pedal. For vehicle longitudinal vehicle speed control, the Lyapunov function is considered as follows.

$$V_1 = \frac{1}{2}S_1^2 \tag{12}$$

after derivation of Lypunov function we can get:

$$\begin{aligned}\dot{V}_1 &= S_1\dot{S}_1 = S_1\left(\dot{x}_1 - \dot{x}_1^r\right)\\ &= S_1\left(x_1x_2x_3 - F_{wind} + \left(F_{Xxd} + F_{Xy}\right)/m_v + d_1 - \dot{x}_1^r\right)\end{aligned} \tag{13}$$

Isokinetic reaching law is selected, which is common adopted in reaching laws.

$$\dot{S}_1 = -K_1 sign(S_1) \tag{14}$$

The reference longitudinal force of vehicle can be obtained.

$$\begin{aligned}F_{Xxd} = -F_{Xy} - \hat{m}_v\Big[-\left(x_1x_2x_3 - F_{wind} - \hat{d}_1 + \dot{x}_1^r\right)\\ - \eta_1 sign(S_1)\Big]\end{aligned} \tag{15}$$

where, $\hat{d}_1$ is the nominal quantity of external interference.

$$\begin{aligned}\dot{V}_1 = S_1\Bigg[\left(1 - \frac{\hat{m}_v}{m_v}\right)x_1x_2x_3 + d_1 - \frac{\hat{m}_v}{m_v}\hat{d}_1 + \left(\frac{\hat{m}_v}{m_v} - 1\right)\dot{x}_1^r\\ - \frac{\hat{m}_v}{m_v}\eta_1 sign(S_1)\Bigg]\end{aligned} \tag{16}$$

The nominal item of vehicle quality is selected as $\hat{m}_v$, so we can get

$$\vartheta_1^{-1} \le \frac{\hat{m}_v}{m_v} \le \vartheta_1,\ \vartheta_1^{-1} = \sqrt{\frac{m_{vmax}}{m_{vmin}}} \ge 1 \tag{17}$$

Define $\hat{\vartheta}_1 = max\left(\left|1 - \vartheta_1^{-1}\right|\ |1 - \vartheta_1|\right)$. The upper limit of external interference is shown as follows.

$$\left|d_1 - \frac{\hat{m}_v}{m_v}\hat{d}_1\right| \le d_{1u} \tag{18}$$

The differential upper limit of vehicle reference state values can be expressed as:

$$\left|\dot{x}_1^r\right| \le \hat{\dot{r}}_1 \tag{19}$$

These two assumptions are reasonable in real vehicle systems with physical constraints from aerodynamic disturbances and vehicle state values from reference models.

$$\dot{V}_1 \le |S_1|\left(\hat{\vartheta}_1\left|x_1x_2x_2\right| + d_{1u} + \dot{\vartheta}_1\hat{\dot{r}}_1 - \frac{\hat{m}_v}{m_v}K_1\right) \tag{20}$$

In order to improve the dynamic quality of the sliding mode, the conditions of the following equation must be satisfied.

$$\dot{V}_1 = |S_1|\frac{d\,|S_1|}{dt} \le -\eta_1\,|S_1| \tag{21}$$

where, η_1 is the design parameter that determines the convergence speed of the sliding mode surface. In order to satisfy the arrival condition of sliding mode control, the parameters in the isokinetic control law must satisfy the following conditions.

$$K_1 > \vartheta_1\left(\hat{\vartheta}_1\left|x_1x_2x_2\right|_{max} + d_{1u} + \hat{\vartheta}_1\hat{\dot{r}}_1 + \eta_1\right) \tag{22}$$

where, $|x_1x_2x_2|_{max}$ $(= \max(|x_1x_2x_2|))$ is the upper limit of the vehicle model. The gain parameter guarantees that the control law satisfies the sliding mode condition with uncertainties of external disturbances and modeling.

The discontinuous sign function sign (S_1) causes chattering phenomenon of the sliding mode motion. Chattering is unfavorable and must be weakened to ensure the normal operation of the controller [12]. Generally, a thin boundary layer near the sliding surface can be used to eliminate the control discontinuity by continuous approximation. Approximate function adopts continuous saturated linear function $\text{sat}(S_1/\Phi_1)$.

$$\begin{aligned}v_1 &= F_{Xxd}\\ &= -F_{Xy} - \hat{m}_v\left[-x_1x_2x_3 + F_{wind} - \hat{d}_1 + \dot{x}_1^{ref} - K_1 sat(S_1/\Phi_1)\right]\end{aligned} \tag{23}$$

The thickness of the thin boundary is Φ_1.

2) STABILITY JUDGMENT CONTROLLER

The sum of r and β is the heading angle of the vehicle, which reflect lateral stability of the vehicle [39]. Whether the vehicle is in stability or not can be judged by the stability judgment controller, which is the fundamental of optimized handling stability strategy. The $\beta - r$ phase portrait provide an effective way to judge vehicle stability and can be described by mathematical methods which has been widely adopted as the vehicle stability judgment in vehicle dynamics research [23]. The $\beta - r$ phase portraits in this study are get by 2DOF-VM and Magic Formula model [24]. The vehicle stability judgment controller is based on $\beta - r$ phase portraits design. The phase portraits $\beta - r$ stability parallelogram boundary lines are

$$\begin{cases}\beta = b_0 r - b_1\\ r = b_3\beta + b_4\\ \beta = b_0 r - b_1\\ r = b_3\beta - b_4\end{cases} \tag{24}$$

The specific values or expressions of parameters can be expressed as follows

$$\begin{aligned}&b_0 = \frac{l_2}{v_x},\ b_1 = \tan\left(\alpha_{s,r}\right),\ b_3 = \frac{r_D - r_C}{\beta_D - \beta_C},\\ &b_4 = r_C - \beta_C b_3,\ r_C = \frac{\mu g}{v_x}\end{aligned} \tag{25}$$

$$r_D = \frac{v_x}{l_1 + l_2}\left(\tan\left(\alpha_{s,f} + \delta_{max}\right) - \tan\left(\alpha_{s,r}\right)\right), \tag{26}$$

$$\beta_C = \frac{l_2 g\mu}{v_x^2} - \tan\left(\alpha_{s,r}\right) \tag{27}$$

$$\beta_D = \frac{l_2}{l_1 + l_2}\left(\tan\left(\alpha_{s,f} + \delta_{max}\right) - \tan\left(\alpha_{s,r}\right)\right) + \tan(\alpha_{s,r})$$

where, δ_{max} is maximum steering angle of front wheel under physical constraints. $\alpha_{s,f}$ and $\alpha_{s,r}$ are tire slip angle of brush tire model, which can be confirmed in [23]. When the vehicle

state is inside the parallelogram, we consider that the vehicle has the handling stability characteristics, otherwise the vehicle does not have stability ability.

3) LATERAL STABILITY CONTROLLER

The lateral stability controller has two control modes, one is an instability control mode, the other is a continuous control mode, both of which are designed for improvement vehicle handling stability. When the vehicle state exceeds the stability region of the envelope parallelogram, the instability control mode is adopted so as to keep the vehicle within its boundaries by exerting an active yaw moment. If the vehicle current state is pushed back to the selected envelope parallelogram stability region as quickly as possible, the sliding surface design should take into account the states error from current states point to envelope's safety closest point, which is defined as a linear combination to the states error.

$$S_2 = x_2 - x_2^s + \Lambda\left(x_3 - x_3^s\right) \tag{28}$$

The point (β, r) represents the current vehicle current states outside the envelope area. $\left(x_{2,}^s x_3^s\right)$ represents the closest point on the safe boundary to the current state point. The parameter Λ is the slope of the straight which is equivalent to $S_2 = 0$ in $\beta - r$ plane and passes through the point on the safety boundary.

In order to calculate the active yaw moment in the instability control mode, the state of the vehicle required here is measured or estimated. Derivation of the sliding surface is related to r and β the constant velocity approach law with saturation function is selected as

$$\dot{S}_2 = \dot{x}_2 - \dot{x}_2^s + \Lambda\left(\dot{x}_3 - \dot{x}_3^s\right) = -K_2 sat\left(S_2/\Phi_2\right) \tag{29}$$

For positive side slip boundary, the active yaw moment can be obtained.

$$\begin{aligned} v_2 = M_{Zxd1} = \frac{\left(1+b_0^2\right) I_z}{b_0^2 + \Lambda b_0}\Bigg[& -K_2 sat\left(\frac{S_2}{\Phi_2}\right) \\ & + \frac{b_0+1}{\left(1+b_0^2\right) m v_x}\left(\mathfrak{J}_1 \boldsymbol{F_x} + \mathfrak{J}_2 \boldsymbol{F_y}\right) \\ & - \frac{2b_0\dot{b}_0 + \Lambda\left(1-b_0^2\right)\dot{b}_0 + (b_0+1)\left(\left(1+b_0^2\right)\right)}{\left(1+b_0^2\right)^2} r \\ & - \frac{b_1\left(1-b_0^2\right)\dot{b}_0}{\left(1+b_0^2\right)^2}\beta - \frac{b_0^2+\Lambda b_0}{\left(1+b_0^2\right)} d_3 - \frac{b_0+1}{\left(1+b_0^2\right)} d_{2} \\ & - \frac{b_1\left(b_0^2-1\right)\dot{b}_0 + 2\Lambda b_0 b_1 \dot{b}_0}{\left(1+b_0^2\right)^2}\Bigg] \end{aligned} \tag{30}$$

If the designed yaw controller makes the system control stable, the following relation must be should first be satisfied

$$K_2 \geq \left(\frac{1}{m_v}\hat{\vartheta}_1 \left|\mathfrak{J}_1 \boldsymbol{F_x} + \mathfrak{J}_2 \boldsymbol{F_y}\right|_{max} + |x_3|_{max} + d_{2u} + \eta_2\right) \tag{31}$$

with

$$\begin{aligned} d_{2u} &\geq \left|\left(d_2 - \hat{d}_2\right) - \Lambda\left(d_3 - \hat{d}_3\right)\right| \\ \left|x_3 + \hat{x}_2^s + \Lambda \hat{x}_3^s\right|_{max} &= max\left(|x_3|_{max}\right). \end{aligned}$$

The active yaw moment applied by other boundaries can be obtained by the same method.

Envelope control is effective to maintain the stability of the vehicle only when the vehicle state exceeds the stability envelope boundary. However, envelope control is not suitable for improving the handling stability of the vehicle in the envelope region of parallelogram stability because of without the active yaw moment applied. The continuous control mode based on feedback control is active when vehicle state in the envelope region. The target lateral force and target yaw moment in vehicle motion are obtained by controlling the side slip angle and yaw rate, respectively, which can control the vehicle tracking the reference state in real time. 2DOF-VM is commonly used as vehicle reference model, which is adopted to obtain the reference yaw rate in this study [17]. The reference yaw rate can be obtained under steady-state steering condition and tire-road adhesion coefficient limitation [37].

$$r_{des} = min\left(\left|G_{rss}\delta_f\right|, \mu g/v_x\right) sign\left(\delta_f\right) \tag{32}$$

where, G_{rss} and δ_f represents the steady gain of the yaw rate and front axle wheel angle, respectively.

There are two commonly methods to obtain the reference side slip angle of the vehicle [37]. Both of them are designed to make the vehicle have better trajectory tracking ability. One is based on 2DOF model and tire-road adhesion limitation, which is the same as the method of obtaining the reference yaw rate.

$$\beta_{des} = min\left(\left|G_{\beta ss}\delta_f\right|, arctan\left(0.02\mu g\right)\right) sign\left(\delta_f\right) \tag{33}$$

Another method is that the side slip angle is set to zero to achieve better trajectory tracking and driver maneuverability, which is suitable for active steering vehicles [27], [31]. The side slip angle of the vehicle is independently controlled and decoupled from the yaw rate. In order to achieve better handling stability and considering 4WIDEV is an overdrive system, the reference side slip angle of the vehicle is set to zero.

$$\beta_{des} = 0 \tag{34}$$

The target lateral force and target yaw moment in vehicle motion are obtained based on feedback control by the way of the side slip angle and yaw rate of the vehicle tracking the reference side slip angle and reference yaw rate, respectively. We select the following sliding surface, in sliding mode control, to achieve the vehicle state tracking reference vehicle state.

$$S_3 = x_2 - x_2^r \tag{35}$$

Control law of sliding surface (S_3) can be obtained.

$$\begin{aligned} v_3^* = F_{Yxd}^* = & -F_{Yy} \\ & + \hat{m}_v v_x\left[x_3 + F_{wind} - \hat{d}_2 + \dot{x}_2^r - K_3 sat\left(\frac{S_2}{\Phi_2}\right)\right] \end{aligned} \tag{36}$$

The Lyapunov arrival condition is satisfied as long as the inequality is satisfied $K_2 \geq \vartheta_1\left(\hat{\vartheta}_1 |x_3|_{max} + d_{3u} + \hat{\vartheta}_1 \hat{r}_2 + \eta_3\right)$.

Where, $|x_1x_3|_{max} = max\ (|x_1x_3|)$. $\left|\dot{x}_2^r\right| \le \hat{\dot{r}}_2$ is the upper limit of reference sideslip angle of vehicle. $\left|d_2 - \hat{d}_2\hat{m}_v \Big/ m_v\right| \le d_{3u}$ is the upper limit of external disturbance.

Similarly, for sliding mode surface S_4:

$$S_4 = x_3 - x_3^r \tag{37}$$

We can get the control law, as described:

$$v_4 = M_{zxd2} = -M_{Zy} + \hat{I}_z\left[-\hat{d}_3 + \dot{x}_3^r - K_4 sat\left(S_4/\Phi_4\right)\right] \tag{38}$$

where, in order to ensure that the sliding surface meets the Lyapunov reaching condition, the inequality $K_3 \ge \vartheta_2\left(d_{4u} + \hat{\vartheta}_2\hat{\dot{r}}_3 + \eta_4\right)$ must be satisfied. $\vartheta_2 = \sqrt{I_{zmax}/I_{zmin}}$, $\hat{\vartheta}_2 = max\left(\left|1 - \vartheta_2^{-1}\right| |1 - \vartheta_2|\right)$, $\left|\dot{x}_3^r\right| \le \hat{\dot{r}}_3$ is the upper limit of reference yaw rate differential. $\left|d_3 - \hat{d}_3 I_z \Big/ I_z\right| \le d_{4u}$ is the upper limit of external interference. And η_4 is also a design parameter that determines the convergence speed of the sliding mode surface.

The continuous control mode has good applicability when the side slip angle is small. However, the applicability of this method becomes worse when the vehicle is in extreme condition. The target lateral force required in vehicle motion becomes larger with the increase of the side slip angle of vehicle, which becomes difficult to satisfy because the lateral force generated by the longitudinal force of the tire is limited especially under extreme conditions.

In order to improve vehicle handling stability, a continuous control mode with adaptive modification of the lateral force is proposed based on phase plane of side slip angle and side slip angle rate, aiming at the saturation problem of motors' torque distribution caused by target lateral force. The phase plane of side slip angle and side slip angle rate of the vehicle ($\beta - \dot{\beta}$ phase plane) [39], which is also commonly used to describe vehicle handling stability, can be described as

$$\left|B_1\dot{\beta} + \beta\right| = B_2 \tag{39}$$

where, B_1 and B_2 are parameters related to tire-road adhesion coefficient, whose values can be referred in [27] in different tire-road adhesion coefficient as depicted in Table 2.

TABLE 2. Parameters value of B_1 and B_2 under different tire-road adhesion coefficient.

Adhesion coefficient	B_1	B_2
$0.8 \le \mu < 1$	0.357	5.573
$0.6 \le \mu < 0.8$	0.357	4.654
$0.4 \le \mu < 0.6$	0.303	4.228
$0.2 \le \mu < 0.4$	0.297	3.345
$\mu < 0.2$	0.284	2.577

Γ is defined as the parameter of stability, which approximately denotes the degree of vehicle handling stability.

$$\Gamma = \begin{cases} 1 - \dfrac{\left|B_1\dot{\beta} + \beta\right|}{B_2} & \left|B_1\dot{\beta} + \beta\right| \le B_2 \\ 0 & \left|B_1\dot{\beta} + \beta\right| > B_2 \end{cases} \tag{40}$$

The greater the value of Γ, the higher the handling stability of the vehicle and vice versa. When the value of Γ is zero, which denotes the vehicle becomes unstable. The target lateral force is modified by the parameter of stability Γ. The target lateral force with adaptive modification as final value of target lateral force.

$$v_3 = F_{Yxd} = \Gamma v_3^* = \Gamma F_{Yxd}^* \tag{41}$$

When the side slip angle of the vehicle becomes larger the value of the target lateral force decreases correspondingly, which is realized by self-adaptive adjustment based on the handling stability degree.

The above is the vehicle motion controller designed. The vehicle's actual speed follows the longitudinal reference speed to obtain the longitudinal force required during vehicle motion. In addition, when the vehicle exceeds the stability boundary through stability judgment by stability judgment controller the yaw moment controller will exert an active yaw moment, so that the vehicle state can return to the stability region again, ensuring the stability of vehicle.

B. VEHICLE TORQUE DISTRIBUTION CONTROLLER

This section mainly introduces vehicle torque distribution controller, whose purpose is to distribute the target longitudinal force and active yaw moment ($\boldsymbol{V}_{d1} = \begin{bmatrix} v_1 & v_2 \end{bmatrix}^T$) or the target longitudinal force, the target lateral force and target yaw moment active yaw moment ($\boldsymbol{V}_{d2} = \begin{bmatrix} v_1 & v_3 & v_4 \end{bmatrix}^T$) obtained by the vehicle motion controller to desired driving or regenerative braking torque of each motor reasonably and effectively. This process is mainly divided into two steps. Firstly, comprehensively considering the amplitude saturation limit of motor torque, friction elliptical circle constraint of tire force, the desired longitudinal force of each tire $\boldsymbol{u}_d = \begin{bmatrix} F_{xd11} & F_{xd12} & F_{xd21} & F_{xd22} \end{bmatrix}^T$ is obtained by tire force distribution controller. Secondly, the desired driving or regenerative braking torque of four wheels T_{dij} can be obtained through by slip ratio controller, which prevents each wheel from excessive slip.

1) TIRE FORCE DISTRIBUTION CONTROLLER

Vehicle longitudinal force F_X, lateral force F_Y and yaw moment M_Z in vehicle motion are produced by tire longitudinal force F_{xij} and tire lateral force F_{yij} as equation described. Because the vehicle does not have active steering condition, the vehicle longitudinal force F_{Xx}, vehicle lateral force F_{Yx} and vehicle yaw moment M_{Zx} generated by tire lateral force F_{yij} cannot be controlled by active intervention through algorithm. The vehicle longitudinal force F_{Xy}, vehicle lateral force F_{Yy} and vehicle yaw moment M_{Zy} generated

by tire longitudinal force F_{xij} can be independently controlled in 4WIDEV. Before the tire force distribution controller, the generalized longitudinal force F_{Xxd}, the generalized lateral force F_{Yxd} and generalized yaw moment M_{Zxd} of the 4WIDEV, which has the following relationship with tire longitudinal force.

$$\begin{aligned} F_{Xxd} &= F_{xd11}\cos\delta_{11} + F_{xd12}\cos\delta_{12} + F_{xd21} + F_{xd21} \\ F_{Yxd} &= F_{xd11}\sin\delta_{11} + F_{xd12}\sin\delta_{12} + F_{xd21} + F_{xd21} \\ M_{Zxd} &= \frac{d}{2}(-F_{xd11}\cos\delta_{11} + F_{xd12}\cos\delta_{12} \\ &\quad - F_{xd21} - F_{xd22}) + l_1(F_{xd11}\sin\delta_{11} + F_{xd12}\sin\delta_{12}) \end{aligned} \tag{42}$$

We establish the relationship between generalized forces/yaw-moment and desired tire longitudinal force.

$$\boldsymbol{V}_d = \boldsymbol{B}\boldsymbol{u}_d \tag{43}$$

Equation (43) has different form when in two different control modes. The generalized matrix $\boldsymbol{V}_d$ is $\boldsymbol{V}_{d1}$, control allocation matrix $\boldsymbol{B}$ is $\boldsymbol{B}_1$ in instability control mode. The generalized matrix $\boldsymbol{V}_d$ is $\boldsymbol{V}_{d2}$ and control allocation matrix $\boldsymbol{B}$ is $\boldsymbol{B}_2$ when in another mode after stability judgment.

$$\begin{aligned} \boldsymbol{B}_1 &= \begin{bmatrix} \cos\delta_{11} & \cos\delta_{12} & 1 & 1 \\ -\frac{d}{2}\cos\delta_{11} + l_1\sin\delta_{11} & \frac{d}{2}\cos\delta_{12} + l_1\sin\delta_{12} & -\frac{d}{2} & \frac{d}{2} \end{bmatrix} \\ \boldsymbol{B}_2 &= \begin{bmatrix} \cos\delta_{11} & \cos\delta_{12} & 1 & 1 \\ \sin\delta_{11} & \sin\delta_{12} & 0 & 0 \\ -\frac{d}{2}\cos\delta_{11} + l_1\sin\delta_{11} & \frac{d}{2}\cos\delta_{12} + l_1\sin\delta_{12} & -\frac{d}{2} & \frac{d}{2} \end{bmatrix} \end{aligned} \tag{44}$$

In addition, the nonlinear saturation constraint conditions of tire force need to be fully considered.

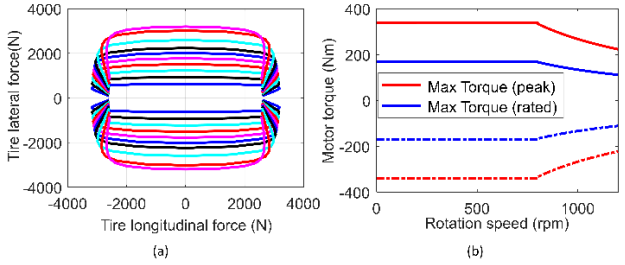

FIGURE 4. Constraints in tire force distribution. (a) Tire friction ellipse circle. (b) Amplitude constraint of in-wheel motor.

As described in Fig. 4(a), The tire longitudinal force and the tire lateral force are coupled and restricted by the road adhesion coefficient and the tire vertical load, which can be described as

$$F_{tij} = \sqrt{\left(\frac{F_{xij}}{C_{xij}}\right)^2 + \left(\frac{F_{yij}}{C_{yij}}\right)^2} \le \mu_{ij}F_{zij} \tag{45}$$

Ignoring the difference between the tire longitudinal force and the tire lateral force $C_{xij} = C_{yij} = 1$, and assuming that the tire is in pure rolling condition, the reference longitudinal force is limited by the peak value.

$$F_{xdij} \le \mu_{xpij}F_{zi} = C_{xij}\mu_{ij}F_{zij} = \mu_{xpij}F_{zij} \tag{46}$$

where, μ_{xpij} is the coefficient of peak lateral force adhesion of tire under pure rolling condition.

The output capacity of the motor also needs to be taken as one constraint. Fig. 4(b) shows the output capacity of in-wheel motor, which clearly described the maximum output torque in two different working modes. The desired longitudinal tire force of four wheels should not exceed the amplitude limit of the corresponding motor.

$$\frac{T_{bmax}}{R_{eff}} \le F_{xdij} \le \frac{T_{dmax}}{R_{eff}} \tag{47}$$

where, T_{bmax} and T_{dmax}, respectively, the maximum braking torque and maximum driving torque of four motors. The above desired longitudinal force solution can be summed up as a control allocation under constraints. R_{eff} is the effective radius of wheel.

$$J = \|\boldsymbol{W}_v(\boldsymbol{B}\boldsymbol{u}_d - \boldsymbol{V}_d)\|_2 \, \boldsymbol{u}_{min} \le \boldsymbol{u}_d \le \boldsymbol{u}_{max} \tag{48}$$

where, $\boldsymbol{W}_v$ is the weight matrix for controlling distribution deviation. The efficient set algorithm is used to solve the constrained optimization problem obtaining the desired longitudinal force of each tire.

2) TIRE SLIP RATIO CONTROLLER

The desired driving and regenerative braking torque T_{dij} got by tire slip ratio controller should considers reference tire longitudinal force F_{xdij} as well as the slip ratio of each wheel s_{ij}. The tire slip ratio control algorithm is described below.

The desired longitudinal force should be considered in calculating the output torque of each motor. They have a direct relationship with each other, which can be obtained by wheel dynamics.

$$T_{dij} = I_w\dot{\omega}_{ij} + F_{dij}R_{eff} \tag{49}$$

where, I_w and ω_{ij} are wheel inertia and angular velocity of each wheel.

Fig. 5 depicts the tire longitudinal force with wheel slip rate changing under several different vertical loads and dry asphalt pavement. Ignoring the difference in vertical load changing and different tire-road adhesion coefficient μ, the optimal slip ratio is the constant value 0.2. In order to ensure the tire longitudinal force output of the vehicle while guarantee enough lateral tire force output capacity, the slip ratio should be limited below the optimal slip ratio.

The expected wheel angular velocity ω_{wdes} can be obtained by the optimal slip ratio s_o differently depending on traction and braking conditions.

$$\omega_{wdes} = \begin{cases} \dfrac{v_x}{R_{eff}(1 - s_o)} & driving \\ \dfrac{v_x(1 - s_o)}{R_{eff}} & brakin \end{cases} \tag{50}$$

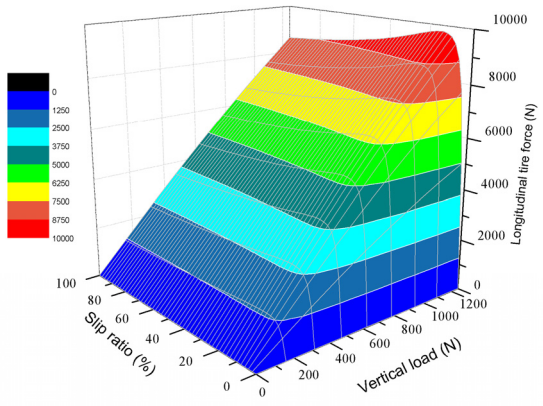

FIGURE 5. Tire force changing with slip ratio.

After determining the wheel slip ratio exceeds the optimal slip ratio s_o, that is to say, the wheel angular velocity ω_{wij} exceeds the boundary of expected wheel angular velocity ω_{wdes}, SMC is applied to generate a modified torque ΔT_{ij}. The sliding surface is defined as follows.

$$S_5 = \omega_w - \omega_{wdes} \tag{51}$$

The sliding surface is defined as a linear error of wheel angular velocity. Sliding condition is defined as follows.

$$\dot{S}_5 = \dot{\omega}_w - \dot{\omega}_{wdes} = -K_5 sign(S_5)\ K_5 > 0$$

Consider the wheel dynamics equation with modified drive or brake torque ΔT_{ij} input.

$$\dot{\omega}_{wij} = \frac{1}{I_w}(T_{dij} - F_{dij}R_{eff}) + \Delta T_{ij} \tag{52}$$

The modified drive or brake torque ΔT_{ij} can be determined.

$$\Delta T_{ij} = -\frac{1}{I_w}(T_{dij} - F_{dij}R_{eff}) + \dot{\omega}_w - ksign(S) \tag{53}$$

The desired driving and regenerative braking torque of each motor T_{dij} can be defined through the above analysis.

$$T_{dij} = \begin{cases} I_w\dot{\omega}_{ij} + F_{dij}R_{eff} & |s| < |s_o| \\ I_w\dot{\omega}_{ij} + F_{dij}R_{eff} + \Delta T_{ij} & |s| \geq |s_o| \end{cases} \tag{54}$$

The motor output torque command is sent to each motor controller to control the planar movement of the vehicle so as to improve the vehicle's handling stability.

IV. SIMULATION

In this section, the control strategy proposed is implemented and evaluated through co-simulation of MATLAB/Simulink and Carsim. The optimized handling stability control strategy is constructed in MATLAB/Simulink and 4WIDEV model with modified structural parameters is built in Carsim. The basic parameters of the vehicle and in-wheel motor are presented in Table 1. The control strategy presented in this study is evaluated compared with 'without stability control', 'automatic switching control' and 'ordinary continuous control' under low tire-road adhesion coefficient at three conditions: single lane change, snake lane change and double lane change, where they are marked, respectively, 'L4', 'L1', 'L2', and 'L3' one after another to facilitate the description of figures later. In fact, 'without stability control' mentioned here actually only has a longitudinal motion controller without lateral stability controller where actual longitudinal speed tracks the reference longitudinal speed of 4WIDEV based on SMC and the average distribution method is adopted to obtain desired torque of each in-wheel motor. 'Automatic switching control' is designed by envelope control in lateral stability controller and do not have a continuous control mode while 'automatic switching control' is a control method, which uses the continuous mode without adaptive parameter adjustment, compared with the control strategy presented. Both of their torque allocation methods remain the same as optimized control strategy's and they are also built in MATLAB/Simulink and use the same vehicle model in Carsim as the proposed control strategy.

A. SINGLE LANE CHANGE

A sine-wave input (2-6s) with the steering wheel angle changing in a period of amplitude 160 degrees is conducted, as shown in Fig. 6(a). The reference longitudinal speed is set to constant value 20 m/s under tire-road condition with adhesion coefficient 0.4. The simulation results for a single lane change maneuver with 15s simulation are shown in Fig. 6 and Fig. 7.

Fig. 6(b)–(f), respectively, shows the vehicle trajectory, longitudinal speed and yaw rate of the vehicle under different control strategies, ''without control strategy'' (L1), ''automatic switching control'' (L2), ''ordinary continuous control'' (L3) and the control strategy proposed in this study (L4). It can be seen from Fig. 6(b) that after 6s steering wheel sine-wave input the vehicle lateral displacement error is smallest, in which its value only reaches 0.56m, when vehicle reaches 300m compared with the vehicle lateral displacement error 15.45m, 7.01m and 2.21m under three other control strategies. In Fig. 6(c), we can be confirmed that under automatic switching control the longitudinal speed of the vehicle fluctuates twice in 5.3 seconds and 3.2 seconds, respectively. The ordinary continuous control strategy and control strategy proposed in this study track the desired yaw rate better than without control strategy and automatic switching control strategy.

Fig. 6(e) and Fig. 6(f) show the $\beta - r$ phase portraits and $\beta - \dot{\beta}$ phase portraits where the parallelogram composed of two of parallel lines represents the stability region in Fig. 6(e). It can be shown that handling stability under the control strategy proposed in this study is improved because it is confined to a stable range and has the smallest phase diagram motion. It also can be seen from Fig. 6(d) that both the without control strategy and automatic switching control strategy exceed the stability boundary of side slip angle and yaw rate phase plane tending to be unstable. There are no

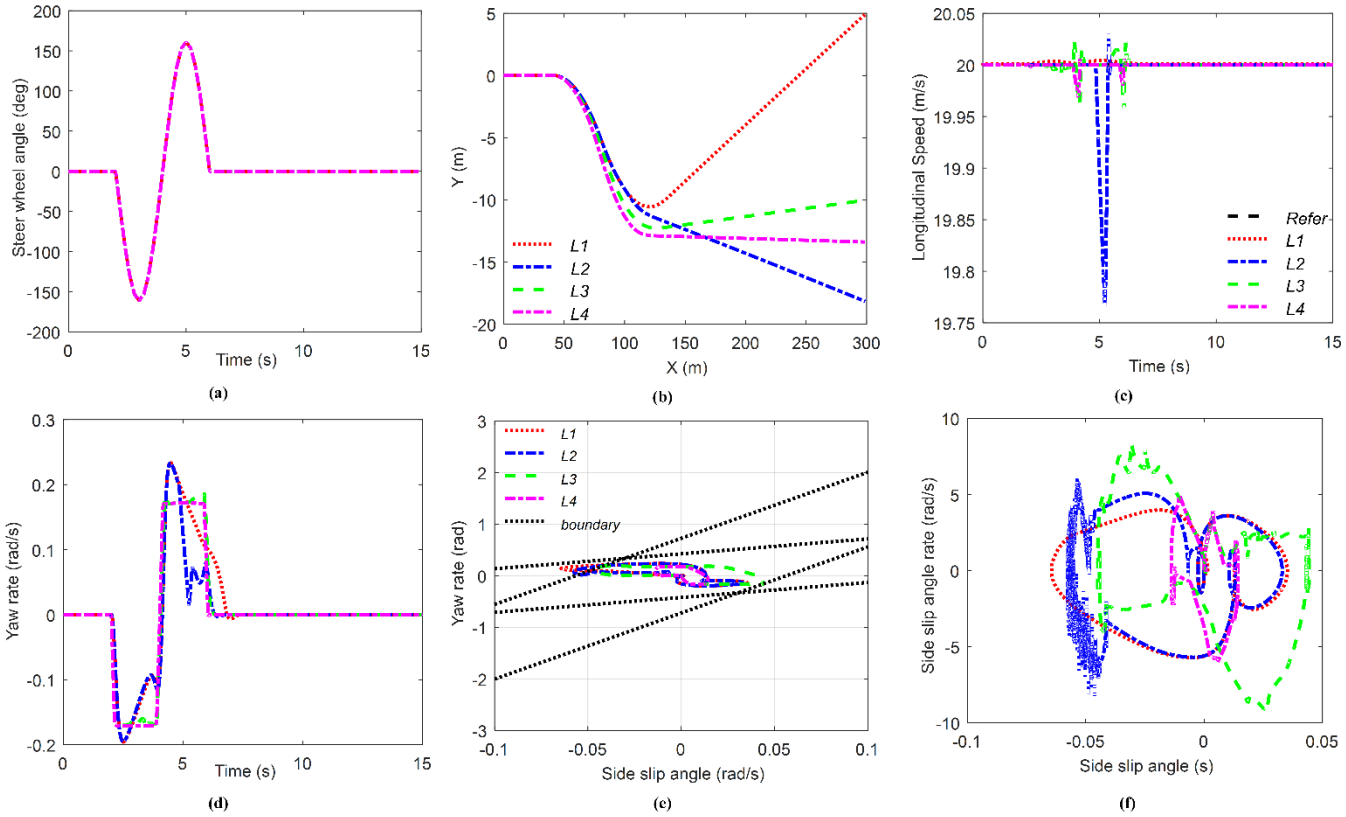

FIGURE 6. Simulation results under four different control strategies. (a) A sine-wave input. (b) Vehicle trajectory. (c) Longitudinal speed. (d) Yaw rate. (e) The $-\beta r$ phase portraits. (f) The $-\beta\dot{\beta}$ phase planes.

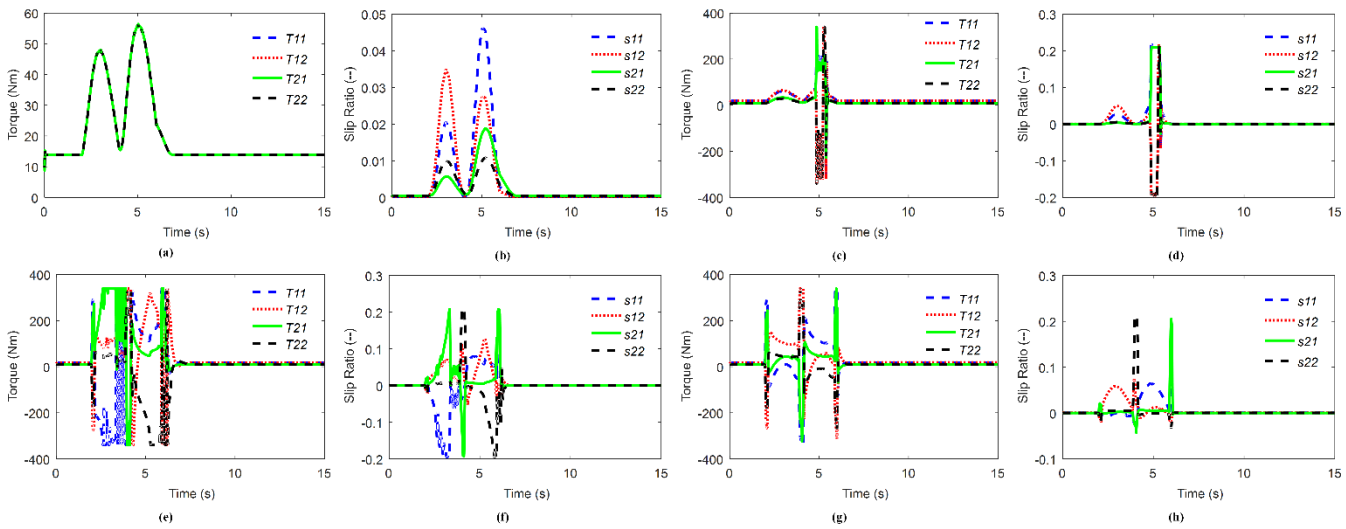

FIGURE 7. Simulation results under four different control strategies. (a) Four motors' torque (L1). (b) Four wheels' slip ratio (L1). (c) Four motors' torque (L2). (d) Four wheels' slip ratio (L2). (e) Four motors' torque (L3). (f) Four wheels' slip ratio (L3). (g) Four motors' torque (L4). (h) Four wheels' slip ratio (L4).

lateral motion and yaw motion control beyond the stability range under without control method.

However, when exceeded the stability boundary under automatic switching control an active yaw moment is applied rapidly, readjusting to the interior of the parallelogram of the phase diagram stability. Yaw rate decreases rapidly (5s) when the active yaw moment is applied and it prevents excessive lateral deviation of the vehicle to a large extent.

Fig. 7(b), (d), (f) and (h), in which s11, s12, s21 and s22 are the slip ratio of front-left, front-right, rear-left and rear-right

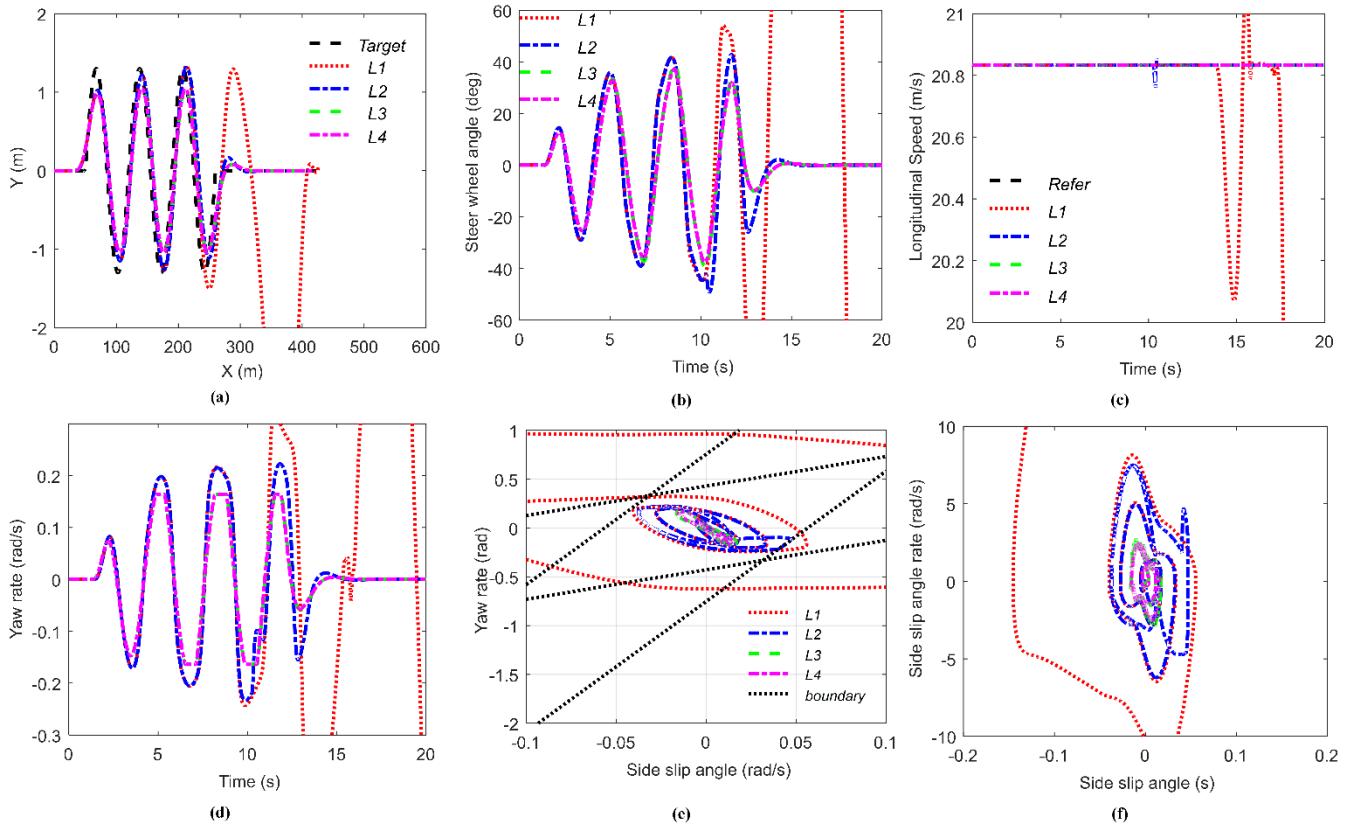

FIGURE 8. Simulation results under four different control strategies. (a) Vehicle trajectory. (b) Driver steering wheel angle. (c) Longitudinal speed. (d) Yaw rate. (e) The $\beta - r$ phase portraits. (f) The $\beta - \dot{\beta}$ phase planes.

wheel, show slip rate can be maintained within a reasonable range under different control strategy. Besides, from description of the number and time of the slip rate of four wheels reaches the optimal slip rate, the proposed control strategy is the best by comparing ordinary continuous control, automatic switching control.

Fig. 7(a), (c), (e) and (g) show the driving and regenerative braking torque under four different control strategies. The output of each electric wheel remains the same as the other because of the average distribution method under without control strategy and cannot make corresponding changes according to the vehicle status changes in real-time. From description in Fig. 7(c), the driving and regenerating braking torque of each electric wheel can be adjusted dynamically in real time to satisfy the active yaw moment required by vehicle motion. For example, the two electric wheels on the left generate driving torque while the two electric wheels on the right generate regenerating braking torque. Compared with the ordinary continuous control strategy, the output of each in-wheel motor of proposed control strategy is more reasonable by dynamically adjusted the proportion of the side slip angle.

B. SNAKE LANE CHANGE

Snake lane change maneuver with driver closed-loop experimental simulation refers to the controllability and stability test procedure for automobiles-Pylon course slalom test of China (GB/T 3223.1-94) to test and verify the effectiveness of proposed control strategy.

The reference speed of vehicle is set to a constant value 75 km/h with the adhesion coefficient of the tire-road 0.4. Fig. 8 and Fig. 9 show co-simulation results for snake lane change with driver closed-loop.

Fig. 8(a)–(d) show the trajectory, steering wheel angel, longitudinal speed and yaw rate in four different control strategies, respectively. As can be seen from the Fig. 8(a)–(c), the vehicle without control strategy lose its stability in 5.3 seconds and fails to track target trajectory and other target state variables. The proposed control strategy and ordinary continuous control strategy can track the target trajectory well and both of them are superior to the automatic switching control algorithm from the analysis in Fig. 8(a).

Fig. 8(e) and Fig. 8(f) shows $\beta - r$ phase portraits and $\beta - \dot{\beta}$ phase portraits, respectively based on several different control strategies. It is obvious that without control algorithm is beyond the stability boundary and cannot track desired trajectory, steering wheel angle and reference longitudinal speed, as described in Fig. 8(e). The other three control strategies can be maintained with the stable parallelogram boundary, and it also can be seen that the envelope of the proposed control strategy is smaller, so it has higher stability than the other two control strategies. It should be mentioned

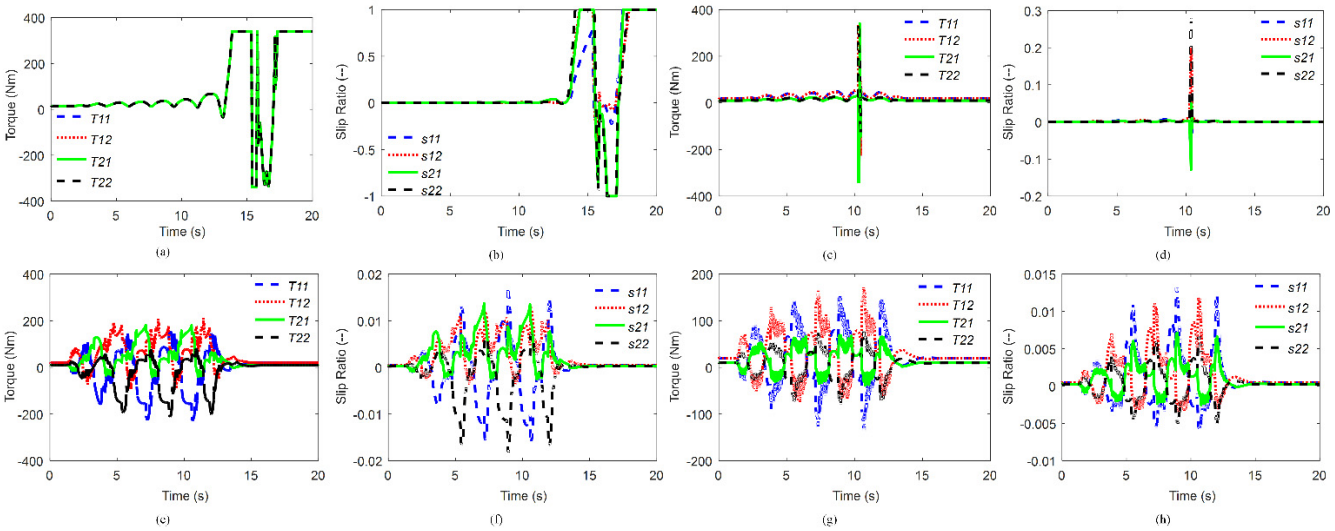

FIGURE 9. Simulation results under four different control strategies. (a) Four motors' torque (L1). (b) Four wheels' slip ratio (L1). (c) Four motors' torque (L2). (d) Four wheels' slip ratio (L2). (e) Four motors' torque (L3). (f) Four wheels' slip ratio (L3). (g) Four motors' torque (L4). (h) Four wheels' slip ratio (L4).

here that here that the automatic switching control is at the envelope boundary at a certain time, which is the result of applying the active yaw moment when vehicle state beyond the envelope of parallelogram stability. This is also the reason that the vehicle loses its stability when the active yaw moment is not applied.

Fig. 9(b), (d), (e) and (h) show the slip ratio of four wheels for the cases without stability control, automatic switching control and the proposed control strategy. In Fig. 9(b), each wheel slipped obviously and the slip ratio reached its maximum after 13 seconds under without control strategy. Fig. 9(d) shows that the slip ratio of automatic switching control algorithm increases instantaneously, exceeding the optimal slip rate at 11s. Ordinary continuous control and the proposed control strategy are relatively small. However, the sliding rate of the control strategy proposed in this study has a smaller variation range, which can be analyzed from the comparison of Fig. 9(f) and Fig. 9(h).

Fig. 9(a), (c), (e) and (f) show the driving or regenerative braking torque of each in-wheel motor, which is the input of vehicle system and determines the control quality. Fig. 9(a) describes that the output torque of each motor without control reaches the maximum saturated amplitude after 11s where over-slip occurs on each wheel. The active yaw moment is satisfied by independent controlling each motor's torque and the vehicle ensures the handling stability when exceeds the envelope of stability and instability will occur. Similarly, by comparing the output torque of four different control strategies, the control strategy proposed has the smallest range, so the theoretical stability theoretically is the largest from the utilization rate of tire force.

C. DOUBLE LANE CHANGE

In this section, International Organization for Standardization passenger cars –test track for a severe lane-change manoeuver (ISO 3888-2:2002) is adopted in double lane change simulation. The road adhesion coefficient is set to 0.2 for road condition setting in the simulation and the reference speed is relatively high constant value 72km/h to verify the effectiveness of vehicle handling stability of the proposed control strategy under limited condition by comparing three other different control strategies.

The experimental simulation results under this condition are illustrated in Fig. 10 and Fig. 11. Fig. 10(a) shows co-simulation results of vehicle motion. Without control strategy and ordinary continuous control strategy cannot track the desired path and fail to maintain vehicle handling stability from described in Fig. 10(a). Both the proposed control strategy and automatic switching control strategy can track the target path and tracking effect of the former is better than that of the latter. As described in Fig. 10(b)–(d), the steering wheel angle, longitudinal speed and yaw rate are consistent with vehicle path analysis.

Fig. 10(e) and Fig. 10(f) show $\beta - r$ phase portraits and $\beta - \dot{\beta}$ phase portraits, respectively. Without control strategy and ordinary continuous control obviously go beyond the envelope of parallelogram stability and the trend of their change is far from the stability region. Both the proposed control strategy and automatic switching control strategy exceed the stability boundary of the parallelogram at a certain time, but return to the stability envelope inside again by applying an active yaw moment.

Fig. 11(b), (d), (f) and (h) show four wheels' slip ratio under four different control strategy. Four wheels slipped excessively, reaching 100% from 12 seconds later without control strategy. The four wheels of ordinary continuous control strategy also start to slip seriously at beginning of 8 seconds where the vehicle began to return to the straight lane again. In addition, rear-right wheel is grievously slipped between 4 and 5 seconds. In the 5 seconds, front-right wheel

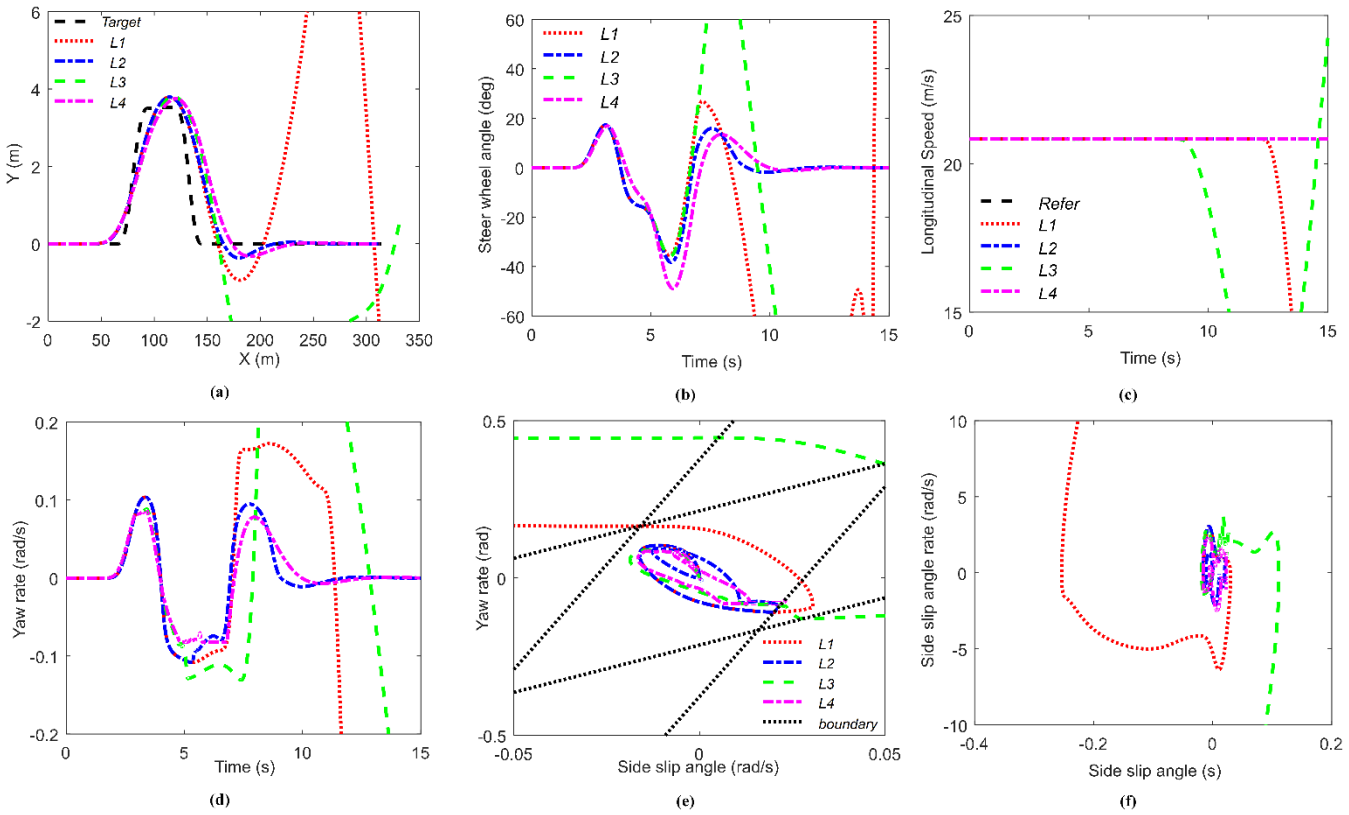

FIGURE 10. Simulation results under four different control strategies. (a) Vehicle trajectory. (b) Driver steering wheel angle. (c) Longitudinal speed. (d) Yaw rate. (e) The $\beta - r$ phase portraits. (f) The $\beta - \dot{\beta}$ phase planes.

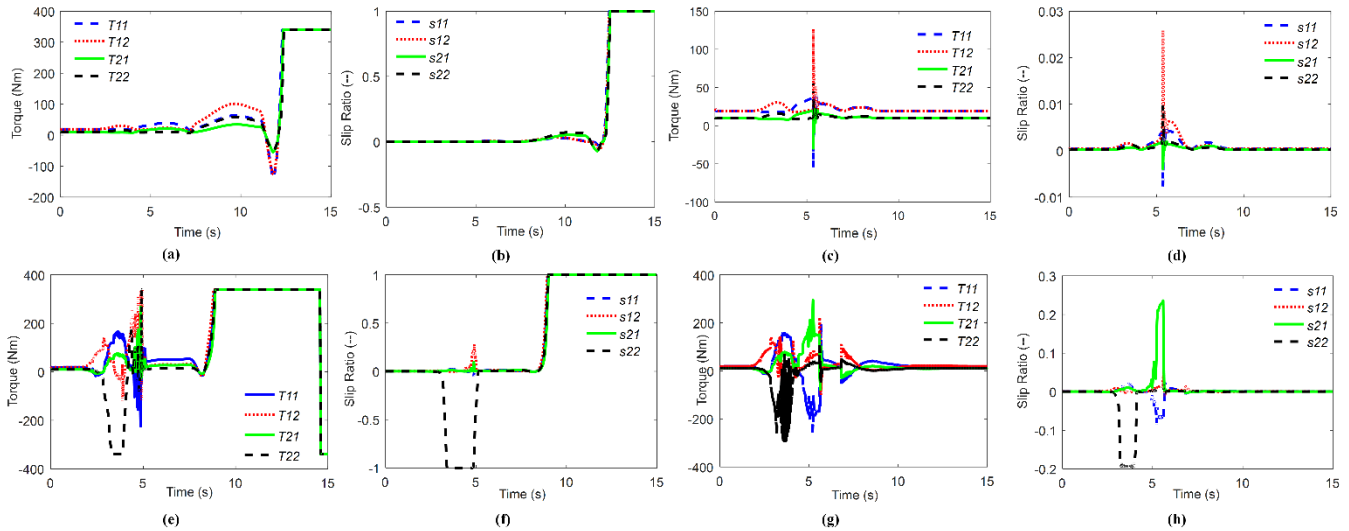

FIGURE 11. Simulation results under four different control strategies. (a) Four motors' torque (L1). (b) Four wheels' slip ratio (L1). (c) Four motors' torque (L2). (d) Four wheels' slip ratio (L2). (e) Four motors' torque (L3). (f) Four wheels' slip ratio (L3). (g) Four motors' torque (L4). (h) Four wheels' slip ratio (L4).

appears pulse fluctuation under automatic switching control strategy. however, the amplitude is still very small (0.02). The slip ratio of four wheels of the proposed control strategy are kept within a relatively small range. Only the right-rear and right-left wheels achieve optimal slip rate twice, respectively.

Fig. 11(a), (c), (e) and (f) describe the four motors' output torques, in which we can also see the control effect under several different control strategies. Without control strategy achieves output saturation limit after 12s, which is caused by lack of lateral and yaw motion control. The motor torque output of automatic switching control, as described

in Fig. 11(c), is in reasonable range. And torque fluctuation of four motors is the results of adjusting vehicle motion by acting the active yaw moment. Fig. 11(e) shows the torque output of four wheels under ordinary continuous control. However, motor saturation is more serious than without control strategy, the reason for which is the target lateral force during vehicle motion needs to be satisfied when torque distribution is carried out. Once the vehicle states exceed the stability range, the target lateral force of the vehicle is difficult to satisfy based on the constant lateral force weight coefficient. The vehicle lateral force produced by the longitudinal force of tire is very small when the vehicle is in the condition of double lane change simulation at low adhesion and high speed. Compared with ordinary continuous control, the proposed control strategy has smaller torque in the stability region, especially the right-rear wheel does not reach saturation by adjusting the weight coefficient of lateral force in real time based on side slip angle and side slip angle rate phase plot.

V. CONCLUSION

The optimized handling stability control strategy proposed in this study for 4WIDEV is co-simulated in MATLAB/Simulink and Carsim. The main conclusions are as follows. The proposed strategy, compared with other control strategies, i.e., without stability control strategy, automatic switching control strategy and ordinary continuous control strategy, can enhance the trajectory following ability under steering wheel input, which is implementation by modifying the weight of generalized lateral force with adjusting the parameter adaptively in the continuous control mode. it also can ensure vehicle handling stability when the vehicle goes beyond the boundary of stability region, which is realization by applying an active yaw moment through instability control mode while maintains each wheel's slip ratio below the optimal slip ratio. The proposed control strategy in this study not only improves the ability of vehicle trajectory following and enhance the handling stability in stability region, but also ensures the handling stability when the vehicle states exceeds the stability region.

REFERENCES

[1] C. Li *et al.*, "An optimal coordinated method for EVs participating in frequency regulation under different power system operation states," *IEEE Access*, vol. 6, pp. 62756–62765, Jun. 2018.

[2] Q. Wang, B. Jiang, B. Li, and Y. Yan, "A critical review of thermal management models and solutions of lithium-ion batteries for the development of pure electric vehicles," *Renew. Sustain. Energy Rev.*, vol. 64, pp. 106–128, Oct. 2016.

[3] Y. Li, B. Li, X. Xu, and X. Sun, "A nonlinear decoupling control approach using RBFNNI-based robust pole placement for a permanent magnet in-wheel motor," *IEEE Access*, vol. 6, pp. 1844–1854, Dec. 2017.

[4] M. A. Hannan, M. S. H. Lipu, A. Hussain, and A. Mohamed, "A review of lithium-ion battery state of charge estimation and management system in electric vehicle applications: Challenges and recommendations," *Renew. Sustain. Energy Rev.*, vol. 78, pp. 834–854, Oct. 2017.

[5] C. Zhang, S. Zhang, G. Han, and H. Liu, "Power management comparison for a dual-motor-propulsion system used in a battery electric bus," *IEEE Trans. Ind. Electron.*, vol. 64, no. 5, pp. 3873–3882, May 2017.

[6] V. Ivanov and D. Savitski, "Systematization of integrated motion control of ground vehicles," *IEEE Access*, vol. 3, pp. 2080–2099, Oct. 2015.

[7] Z. Shuai, H. Zhang, J. Wang, J. Li, and M. Ouyang, "Combined AFS and DYC control of four-wheel-independent-drive electric vehicles over CAN network with time-varying delays," *IEEE Trans. Veh. Technol.*, vol. 63, no. 2, pp. 591–602, Feb. 2014.

[8] R. Wang, C. Hu, Z. Wang, F. Yan, and N. Chen, "Integrated optimal dynamics control of 4WD4WS electric ground vehicle with tire-road frictional coefficient estimation," *Mech. Syst. Signal Process.*, vols. 60–61, pp. 727–741, Aug. 2015.

[9] R. Wang and J. Wang, "Passive actuator fault-tolerant control for a class of overactuated nonlinear systems and applications to electric vehicles," *IEEE Trans. Veh. Technol.*, vol. 62, no. 3, pp. 972–985, Mar. 2013.

[10] D. Zhang, G. Liu, H. Zhou, and W. Zhao, "Adaptive sliding mode fault-tolerant coordination control for four-wheel independently driven electric vehicles," *IEEE Trans. Ind. Electron.*, vol. 65, no. 11, pp. 9090–9100, Nov. 2018.

[11] H. Zhang and J. Wang, "Active steering actuator fault detection for an automatically-steered electric ground vehicle," *IEEE Trans. Veh. Technol.*, vol. 66, no. 5, pp. 3685–3702, May 2017.

[12] H. Liu, Z. Hu, Y. Song, and J. Lin, "Decentralized vehicle-to-grid control for primary frequency regulation considering charging demands," *IEEE Trans. Power Syst.*, vol. 28, no. 3, pp. 3480–3489, Aug. 2013.

[13] B. Zhao, N. Xu, H. Chen, K. Guo, and Y. Huang, "Stability control of electric vehicles with in-wheel motors by considering tire slip energy," *Mech. Syst. Signal Process.*, vol. 118, pp. 340–359, Mar. 2019.

[14] K. Nam, H. Fujimoto, and Y. Hori, "Lateral stability control of in-wheel-motor-driven electric vehicles based on sideslip angle estimation using lateral tire force sensors," *IEEE Trans. Ind. Electron.*, vol. 61, no. 5, pp. 1972–1985, Sep. 2012.

[15] Z. Shuai, H. Zhang, J. Wang, J. Li, and M. Ouyang, "Lateral motion control for four-wheel-independent-drive electric vehicles using optimal torque allocation and dynamic message priority scheduling," *Control Eng. Signal Pract.*, vol. 24, pp. 55–66, Mar. 2014.

[16] H. Alipour, M. Sabahi, and M. B. B. Sharifian, "Lateral stabilization of a four wheel independent drive electric vehicle on slippery roads," *Mechatronics*, vol. 30, pp. 275–285, Sep. 2015.

[17] T. Goggia *et al.*, "Integral sliding mode for the torque-vectoring control of fully electric vehicles: Theoretical design and experimental assessment," *IEEE Trans. Veh. Technol.*, vol. 64, no. 5, pp. 1701–1715, May 2015.

[18] B. Li, A. Goodarzi, A. Khajepour, S.-K. Chen, and B. Litkouhi, "An optimal torque distribution control strategy for four-independent wheel drive electric vehicles," *Vehicle Syst. Dyn.*, vol. 53, no. 8, pp. 1172–1189, May 2015.

[19] C. G. Bobier and J. C. Gerdes, "Staying within the nullcline boundary for vehicle envelope control using a sliding surface," *Vehicle Syst. Dyn.*, vol. 51, no. 2, pp. 199–217, Feb. 2013.

[20] J. Ni, J. Hu, and C. Xiang, "Envelope control for four-wheel independently actuated autonomous ground vehicle through AFS/DYC integrated control," *IEEE Trans. Veh. Technol.*, vol. 66, no. 11, pp. 9712–9726, Nov. 2017.

[21] S. M. Erlien, S. Fujita, and J. C. Gerdes, "Shared steering control using safe envelopes for obstacle avoidance and vehicle stability," *IEEE Trans. Intell. Transp. Syst.*, vol. 17, no. 2, pp. 441–451, Feb. 2016.

[22] L. Yuan, H. Zhao, H. Chen, and B. Ren, "Nonlinear MPC-based slip control for electric vehicles with vehicle safety constraints," *Mechatronics*, vol. 38, pp. 1–15, Sep. 2016.

[23] L. Zhai, T. Sun, and J. Wang, "Electronic stability control based on motor driving and braking torque distribution for a four in-wheel motor drive electric vehicle," *IEEE Trans. Veh. Technol.*, vol. 65, no. 6, pp. 4726–4739, Jun. 2016.

[24] R. Wang, H. Zhang, J. Wang, F. Yan, and N. Chen, "Robust lateral motion control of four-wheel independently actuated electric vehicles with tire force saturation consideration," *J. Franklin Inst., Eng. Appl. Math.*, vol. 352, no. 2, pp. 645–668, Feb. 2015.

[25] G. Yin, R. Wang, and J. Wang, "Robust control for four wheel independently-actuated electric ground vehicles by external yaw-moment generation," *Int. J. Automot. Technol.*, vol. 16, no. 5, pp. 839–847, Oct. 2015.

[26] M. Liu, J. Huang, and M. Cao, "Handling stability improvement for a four-axle hybrid electric ground vehicle driven by in-wheel motors," *IEEE Access*, vol. 6, pp. 2668–2682, Dec. 2018.

[27] H. Jing, F. Jia, and Z. Liu, "Multi-objective optimal control allocation for an over-actuated electric vehicle," *IEEE Access*, vol. 6, pp. 4824–4833, Jan. 2018.

[28] D. Kasinathan, A. Kasaiezadeh, A. Wong, A. Khajepour, S.-K. Chen, and B. Litkouhi, "An optimal torque vectoring control for vehicle applications via real-time constraints," *IEEE Trans. Veh. Technol.*, vol. 65, no. 6, pp. 4368–4378, Jun. 2016.
[29] Z. Wang, C. Qu, L. Zhang, X. Xue, and J. Wu, "Optimal component sizing of a four-wheel independently-actuated electric vehicle with a real-time torque distribution strategy," *IEEE Access*, vol. 6, pp. 49523–49536, Feb. 2018.
[30] L. Chen, T. Chen, X. Xu, Y. Cai, H. Jiang, and X. Sun, "Multi-objective coordination control strategy of distributed drive electric vehicle by orientated tire force distribution method," *IEEE Access*, vol. 6, pp. 69559–69574, Oct. 2018.
[31] W. Liu, H. He, F. Sun, and J. Lv, "Integrated chassis control for a three-axle electric bus with distributed driving motors and active rear steering system," *Vehicle Syst. Dyn.*, vol. 55, no. 5, pp. 601–625, May 2017.
[32] A.-T. Nguyen, C. Sentouh, and J.-C. Popieul, "Sensor reduction for driver-automation shared steering control via an adaptive authority allocation strategy," *IEEE/AMSM Trans. Mechatronics*, vol. 23, no. 1, pp. 5–16, Feb. 2018.
[33] A. M. Dizqah, B. Lenzo, A. Sorniotti, P. Gruber, S. Fallah, and J. De Smet, "A fast and parametric torque distribution strategy for four-wheel-drive energy-efficient electric vehicles," *IEEE Trans. Ind. Electron.*, vol. 63, no. 7, pp. 4367–4376, Jul. 2016.
[34] J. Guo, Y. Luo, K. Li, and Y. Dai, "Coordinated path-following and direct yaw-moment control of autonomous electric vehicles with sideslip angle estimation," *Mech. Syst. Signal Process.*, vol. 105, pp. 183–199, May 2018.
[35] T. Chen, X. Xu, L. Chen, H. Jiang, Y. Cai, and Y. Li, "Estimation of longitudinal force, lateral vehicle speed and yaw rate for four-wheel independent driven electric vehicles," *Mech. Syst. Signal Process.*, vol. 101, pp. 377–388, Feb. 2018.
[36] P. Hang, X. Chen, S. Fang, and F. Luo, "Robust control for four-wheel-independent-steering electric vehicle with steer-by-wire system," *Int. J. Automot. Technol.*, vol. 18, no. 5, pp. 785–797, Oct. 2017.
[37] R. Wang, C. Hu, F. Yan, and M. Chadli, "Composite nonlinear feedback control for path following of four-wheel independently actuated autonomous ground vehicles," *IEEE Trans. Intell. Transp. Syst.*, vol. 17, no. 7, pp. 2063–2074, Jul. 2016.
[38] V. I. Utkin, "Sliding mode control design principles and applications to electric drives," *IEEE Trans. Ind. Electron.*, vol. 40, no. 1, pp. 23–36, Feb. 1993.
[39] X. Xie, L. Jin, Y. Jiang, and B. Guo, "Integrated dynamics control system with ESC and RAS for a distributed electric vehicle," *IEEE Access*, vol. 6, pp. 18694–18704, Apr. 2018.

YONG CHEN received the M.E. degree in mechanical engineering from the Beijing Institute of Technology, Beijing, China, in 2018, where he is currently pursuing the Ph.D. degree with the School of Mechanical Engineering.

His research interests include electric vehicles, pilotless automobiles, vehicle dynamic control, and machine learning.

SIZHONG CHEN received the M.S. degree from the College of Automotive Engineering, Jilin University, Beijing, China, in 1987. He is currently a Professor with the School of Mechanical Engineering, Automotive Research Institute, Beijing Institute of Technology. His current research interests include suspension dynamics and steering, vehicle design, and control technology. He serves as the Secretary General for the SUV Technology Committee of the Society of Automotive Engineering of China.

YUZHUANG ZHAO received the Ph.D. degree from the School of Mechanical Engineering, Beijing Institute of Technology, Beijing, China, in 2011. He is currently an Associate Professor with the School of Mechanical Engineering, Automotive Research Institute, Beijing Institute of Technology. His main research areas include vehicle dynamics and control, continuous damping regulation of semi-active suspension, and vehicle height control strategy for air suspension and hydro-pneumatic suspension.

ZEPENG GAO received the M.S. degree from the School of Mechanical Engineering, Beijing Institute of Technology, Beijing, China, in 2017, where he is currently pursuing the Ph.D. degree. His main research area is vehicle dynamics theory and control, which includes air suspension height adjustment and application of vehicle system vibration energy recovery technology and intelligent control algorithm in vehicle dynamics.

CHANGLONG LI received the B.S. degree in engineering mechanics from Hunan University, Changsha, in 2018. He is currently a Graduate Student with the School of Mechanical Engineering, Beijing Institute of Technology. He is involved in research in area of signal identification, focusing on applying deep learning networks in the field.